

Reports

Todorokites: A New Family of Naturally Occurring Manganese Oxides

Abstract. *Todorokites are found in numerous terrestrial deposits and are important copper- and nickel-bearing materials in manganese nodules. Their structures are highly disordered, not well known, and controversial. High-resolution transmission electron microscopy reveals that terrestrial todorokites consist of tunnel structures of previously unreported dimensions and that these tunnel structures are intergrown coherently on a unit cell scale. Many types and degrees of disorder are evident in the high-resolution images. These newly discovered structures indicate a need for a revised nomenclature of tunnel manganese oxides, and such a system is suggested.*

Todorokites are calcium-bearing manganese oxides found in terrestrial manganese ore deposits, in weathering products of manganese-bearing rocks, and in some manganese nodules. They are, in many cases, major constituents of the manganese nodules (1) and host copper and nickel within the nodules in potentially economic quantities. Knowledge of todorokites is important for understanding how nodules form and how they concentrate transition elements from ocean waters.

Todorokites have been the subject of fairly vigorous controversy. Formerly thought to be a single phase, todorokite was discredited as a mineral by the International Mineralogical Association Commission on New Minerals and Mineral Names in 1970 when evidence was submitted showing it to be a complex mixture of several compounds (2). Many mineralogists, however, felt that this decision was incorrect since recognizable x-ray diffraction patterns could be produced from todorokite collected from

widespread deposits (1). If one assumes that todorokite exists as a distinct species, there is dispute about its structure because x-ray patterns have not been adequate for structure determination. Further confusion is caused by the variable morphology of todorokite, which appears fibrous in some samples and platy in others. We have found todorokite material to have a range of related structures and so refer to it in the plural in the remainder of this report.

In earlier studies, unit cell parameters were derived for todorokites from x-ray powder patterns. Straczek *et al.* (3) found parameters of $a = 9.75 \text{ \AA}$, $b = 2.84 \text{ \AA}$, $c = 9.59 \text{ \AA}$, and $\beta = 90^\circ$ for a unit cell with either orthorhombic or monoclinic symmetry. Faulring (4) found similar parameters of $a = 9.65 \text{ \AA}$, $b = 10.29 \text{ \AA}$, and $c = 2.84 \text{ \AA}$ with α , β , and γ angles varying slightly from 90° for a sample from Charco Redondo, Cuba. The unit cell was considered to be pseudo-orthorhombic and triclinic.

Recent work has been done on todorokites by a variety of techniques. Chukhrov *et al.* (5) have used transmission electron microscopy (TEM) to investigate both terrestrial and marine todorokites. In their electron diffraction patterns they found three types of todorokites with $a = 4.88 \text{ \AA} \times n$ ($n = \text{integer}$). They also found that todorokites commonly form trillings, leading to pseudo-hexagonal diffraction patterns. Potter and Rossman (6) have studied a variety of tetravalent manganese oxides with infrared spectroscopy. The spectra obtained from todorokites were interpreted as resulting from either a layer structure or a chain or tunnel structure of wide dimensions. Burns and Burns (7) favored the tunnel structure interpretation on the basis of morphological and chemical data. They suggested a structure similar to that of the minerals hollandite and romanèchite, and our work confirms their predictions.

Our method of investigation was high-resolution transmission electron microscopy (HRTEM). We used a slightly modified JEOL JEM 100B microscope (7, 8) to study samples from eight localities (9). Samples were ground, suspended in acetone, and deposited on holey carbon grids. Owing to the morphology of the crushed grains, this method allowed viewing only perpendicular to the tunnels. Ion milling of epoxy-impregnated samples was attempted to overcome this problem. The method was successful for the sample from Charco Redondo, Cuba, and for this sample we were able to view down the tunnels.

We found that the structures of to-

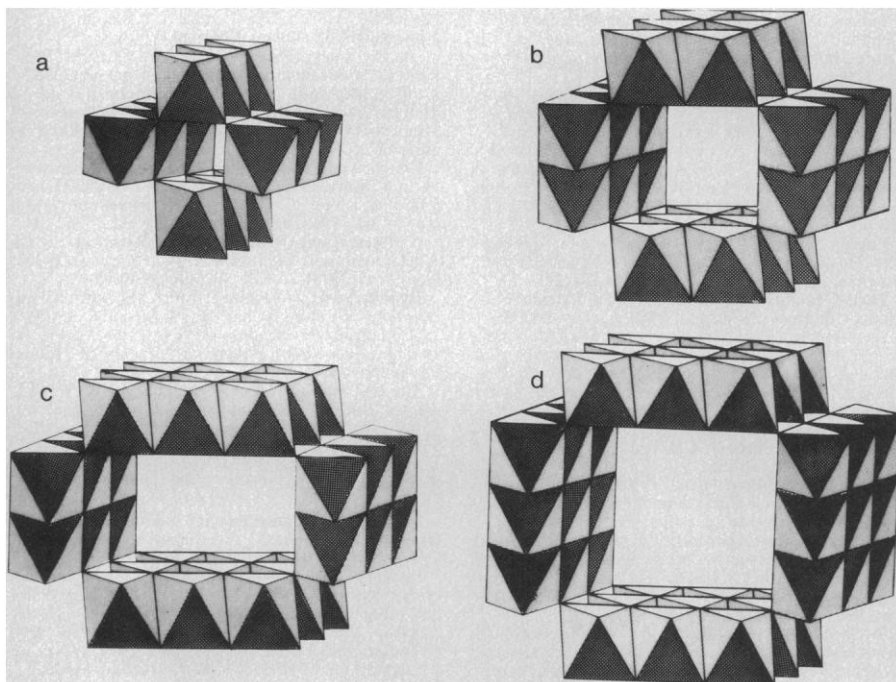


Fig. 1. Diagram of various manganese oxide tunnel structures: (a) 1×1 , pyrolusite; (b) 2×2 , hollandite; (c) 2×3 , romanèchite; and (d) 3×3 , a common member of the todorokite family. Numbers refer to the widths of the manganese octahedral chains around the central tunnels. Large cations and water can be accommodated in the hollandite, romanèchite, and todorokite tunnels.

Table 1. Partial nomenclature scheme for manganese oxide structures.

Family name	Common dimension (m)	Variable dimension (n)				Sheeted end-member ($n \rightarrow \infty$)
		$n = 1$	$n = 2$	$n = 3$	$n = 4$	
Nsutite	1	$T(1, 1)$	$T(1, 2)$	$T(1, 3)$	$T(1, 4) \dots$	
Hollandite-romanèchite	2	$T(2, 1)$	$T(2, 2)$	$T(2, 3)$	$T(2, 4) \dots$	Birnessite
Todorokites	3	$T(3, 1)$	$T(3, 2)$	$T(3, 3)$	$T(3, 4) \dots$	Buserite

match these to experimental images (14). This technique may allow the tunnel contents of todorokites to be deduced by a comparison of experimental images with images computed from variously modeled tunnel contents; however, we have not yet attempted such comparisons.

The nature of the octahedral framework of todorokites is expected to be similar to that of romanèchite (15). Both contain manganese cations in two oxidation states, Mn^{2+} and Mn^{4+} . Romanèchite has three distinct octahedral sites designated M1, M2, and M3 (15). The M1 and M3 sites have average metal-oxygen distances of 1.91 Å. The M2 site has larger metal-oxygen distances of 1.98 Å, and it is therefore in this site that the larger Mn^{2+} cations are presumed to reside (15). In romanèchite, the M2 sites are located along the edges of the triple chains. It is expected that similar segregations of octahedral sites according to oxidation state will be found to occur in todorokites.

Many types of disorder are present in the todorokites. The ubiquity of disorder explains the confusing x-ray diffraction patterns and hence the difficulty in determining structural types by x-ray diffraction measurements. The apparently random fashion of intergrowth of differently sized tunnel structures results in the streaking of diffraction patterns; diffuse diffraction spots occur if one tunnel type is sufficiently prominent. The disordered intergrowth sequences are themselves not consistent over even small areas of the crystal. For example, on the left side of Fig. 3, a 533 sequence changes to a 3232 sequence. This type of disruption is common in the Charco Redondo sample. There are also variants of the individual tunnel structures themselves. For example, the 3×5 tunnels of Fig. 3 are not simple rectangular boxes but have chains of manganese octahedra that diagonally crosscut the centers of the tunnels. This may reflect a necessity for added support in larger tunnel structures.

On a larger scale, twinning is prevalent in the majority of specimens. The twinning occurs in trillings of crystals orient-

ed at 120° angles from one another. In some sample fragments, the twinning occurs on a relatively coarse scale (Fig. 4a), similar to that described by Chukhrov *et al.* (5). In other sample fragments, twinning occurs on a fine scale (Fig. 4b), giving grains a micaceous appearance at low magnifications and a tweedy texture in the high-resolution images. Thus a wide variation in morphology is possible. Untwinned todorokite intergrowths appear fibrous. At the other extreme, samples with the small-scale twinning of Fig. 4b appear platy.

In this study we have looked only at terrestrial samples of todorokites. However, todorokites have also been shown to occur in the cores, fissures, and voids of marine manganese nodules (5, 16, 17). Some examples of manganese nodule todorokites gave diffraction patterns (5) with spacings of 9.75 Å, 14.6 Å, and 24.4 Å predominating in different samples. On the basis of our study, we interpret these spacings to reflect predominant tunnel sizes of 3×3 , 3×5 , and 3×9 , respectively, for these todorokites. It will be of interest to image similar marine specimens by viewing down the tunnel direction, thereby testing our interpretation.

A correlation exists between the presence of todorokite and high concentrations of copper and nickel in deep-sea nodules (16). As postulated by Burns and Burns (1), it seems probable that the smaller transition elements substitute for Mn^{2+} in the octahedral framework. Water and larger atoms such as sodium, calcium, barium, and potassium would then occur in the todorokite tunnels. Future work should be directed toward determining whether the size of todorokite tunnels and the amount of copper and nickel are correlated, and if they reflect the environment of formation of nodules.

In the course of this study, it has become apparent that a revised nomenclature is needed for the new structures of the todorokite family and, indeed, for the whole group of manganese oxide tunnel materials. A detailed discussion of nomenclature is being prepared. A slightly

abbreviated version is given in Table 1 (18), where T denotes a tunnel structure and the dimensions of the tunnel follow in parentheses (m, n). The dimension that is the basis for intergrowth is listed first within the parentheses. Thus the hollandite-romanèchite family is represented as $T(2, n)$, where $n = \text{integer}$. The todorokite family is represented as $T(3, n)$. In this system there is a distinction between $T(m, n)$ and $T(n, m)$, depending upon the intergrowth family in which the tunnel structure occurs. Although tunnel structures characterized as $T(1, n)$, $n > 1$, have not yet been found, it seems probable that they will occur in the nsutite family. As n increases, a layer structure is approached in the two families that contain supporting cations. The end-member of the $T(2, n)$ family as $n \rightarrow \infty$ is possibly birnessite, whereas the end-member of the $T(3, n)$ family as $n \rightarrow \infty$ is possibly buserite. It follows that intergrowths of very wide chain structures (essentially layers) with smaller tunnel structures are possible, although they have yet to be recognized.

SHIRLEY TURNER

Department of Geology,
Arizona State University,
Tempe 85281

PETER R. BUSECK

Departments of Geology and Chemistry,
Arizona State University

References and Notes

- R. G. Burns and V. M. Burns, in *Marine Minerals*, R. G. Burns, Ed. (LithoCrafters, Chelsea, Mich., 1979), pp. 1-46; in *Marine Manganese Deposits*, G. P. Glasby, Ed. (Elsevier, Amsterdam, 1977), pp. 185-248; *Philos. Trans. R. Soc. London* **285**, 249 (1977).
- M. H. Hey and P. G. Embrey, *Mineral. Mag.* **39**, 903 (1974).
- J. A. Straczek, A. Horen, M. Ross, C. M. Warshaw, *Am. Mineral.* **45**, 1174 (1960).
- G. M. Faulring, in *Advances in X-Ray Analysis*, M. Mueller, Ed. (Plenum, New York, 1962), vol. 5, pp. 117-126.
- F. V. Chukhrov, A. I. Gorshkov, A. V. Sivtsov, V. V. Berezovskaya, *Izv. Akad. Nauk SSSR Ser. Geol.* **12**, 86 (1978); *Nature (London)* **278**, 631 (1979).
- R. M. Potter and G. R. Rossman, *Am. Mineral.* **64**, 1199 (1979).
- P. R. Buseck and S. Iijima, *ibid.* **59**, 1 (1974).
- D. R. Veblen, P. R. Buseck, C. W. Burnham, *Science* **198**, 359 (1977); *Am. Mineral.* **64**, 687 (1979).
- Charco Redondo, Cuba; Ambollas, Pyrénée Mountains; Bombay, India; Mamatwan Mine, Hotazel, South Africa; Todoroki Mine, Hakkaido, Japan, U.S. National Museum (USNM) sample 105391; Kuruman, South Africa, USNM 15434; Montenegro, Oriente Province, Cuba, USNM 113967; Santiago, Cuba, USNM 74759.
- S. Turner and P. R. Buseck, *Geol. Soc. Am. Abstr. Programs* **11**, 531 (1979).
- The name psilomelane has also been applied to this mineral. The International Mineralogical Association Commission on New Minerals and Mineral Names voted in August 1969 to make romanèchite the name for the specific mineral and psilomelane a general term for hard, massive botryoidal accretions of manganese oxides.
- S. Turner and P. R. Buseck, *Science* **203**, 456 (1979).
- G. Butler and H. R. Thirsk, *Acta Crystallogr.* **5**, 288 (1952).
- M. A. O'Keefe, P. R. Buseck, S. Iijima, *Nature (London)* **274**, 322 (1978).
- A. D. Wadsley, *Acta Crystallogr.* **6**, 433 (1953).

16. V. M. Burns and R. G. Burns, *Earth Planet. Sci. Lett.* **39**, 341 (1978); *Scanning Electron Microsc.* **1**, 245 (1978); *Am. Mineral.* **63**, 827 (1978).
17. M. Siegel, *Geol. Soc. Am. Abstr. Programs* **11**, 516 (1979).
18. The mineral ramsdellite (MnO₂) is included in the expanded version.
19. We thank D. Davis, J. Post, and D. Veblen for valuable discussion; V. Burns, S. Crane, G. Rossman, and the Smithsonian Institution for

kindly supplying samples for this project; and J. Wheatley for assistance in the electron microscope laboratory in the Center for Solid State Science at Arizona State University. The research was supported in part by grants EAR 77-00128 and EAR 79-26375 from the Earth Sciences Division of the National Science Foundation.

17 June 1980; revised 5 September 1980

Erosion of Galilean Satellite Surfaces by Jovian Magnetosphere Particles

Abstract. *The Galilean satellites of Jupiter—Io (J1), Europa (J2), Ganymede (J3), and Callisto (J4)—are embedded in the intense ion and electron fluxes of the Jovian magnetosphere. The effect of these particles on the icy surfaces of the outer three satellites depends on the fluxes and the efficiency of the sputtering of water ice by such particles. Recent laboratory measurements provided data on the erosion of water ice by energetic particles and showed that it occurs much faster than would be expected from normal sputtering theory. The Voyager spacecraft encounters with Jupiter provided the first measurements of ion fluxes (energies ≥ 30 kiloelectron volts) in the vicinity of the Galilean satellites. Using the laboratory sputtering data together with particle measurements from the Voyager 1 low-energy charged particle experiment, the effects of erosion on the surfaces of J2 to J4 are estimated. It is shown that the surface of Europa could be eroded by as much as 100 meters over an eon (10^9 years). Column densities of water vapor that could be produced around the three satellites from particle bombardment of their surfaces are also calculated, and the sources and losses of oxygen in the gravitationally bound gas produced by sputtering or sublimation are estimated.*

The outer three Galilean satellites of Jupiter—Europa (J2), Ganymede (J3), and Callisto (J4)—are immersed deeply in the magnetosphere of the planet (1, 2). Reflectance spectra show the surfaces of these three satellites to be covered totally or partially with water ice (3). If there is no appreciable atmosphere or intrinsic magnetic field associated with any of the satellites, the charged particles that impact them will produce erosion of their surfaces. Considerations of this erosion process, as well as the erosion of ice grains in the interplanetary and interstellar media, led to the initiation of laboratory experiments to investigate the sputtering of water ice by charged particles. The surprising discovery was made that the erosion was far greater than expected on the basis of contemporary sputtering theory that successfully accounts for erosion of metallic surfaces (4). These early laboratory results were used, together with extrapolations (to lower energies) of the particle fluxes reported from the Pioneer 10 encounter with Jupiter, to estimate the ice removal rates from the Galilean satellite surfaces and the possible satellite atmospheric and magnetospheric effects associated with this removal (5). It was concluded that sputtering played a role at least comparable to that of other erosion processes.

The laboratory experiments on the

sputtering of water ice have been extended to lower energies (6) and possible mechanisms involved in the sputtering process have been discussed to explain the observed species, energy, and temperature dependence. These new laboratory results are used in this report, together with particle energy spectra measured by the low-energy charged particle (LECP) experiment (7) on Voyager 1, to provide substantially more accurate estimates of the expected erosion of the water ice-covered surfaces of the Galilean satellites.

Results from Earth-based observations and from instruments on Voyager 1 and Voyager 2 show the outer three Galilean satellites to have vastly different surface characteristics. Callisto is approximately 5 to 25 percent ice-covered (3, 8) and heavily cratered (9). Ganymede is 20 to 65 percent ice-covered (3) and less cratered than Callisto, with some linear surface features. Europa is nearly 100 percent ice-covered (3), crisscrossed by linear features, and essentially devoid of craters (9). The ice temperatures of Europa and Ganymede have been estimated as ~ 95 and ~ 103 K (10), respectively, substantially colder than the full-disk brightness temperatures of ~ 124 and 135 K, respectively (11). In this report we consider these upper and lower limits on the average

temperatures. The characteristics of the surface of J2 may result from the Galilean satellite equivalent of tectonic processes. However, aspects of the smooth surface may also result from particle bombardment of the surface, as noted by the Voyager 2 imaging experiment team (9) and discussed below.

During the interval when Voyager 1 crossed the orbit planes of the Galilean satellites, the LECP experiment was in its planetary near-encounter mode in order to measure the most intense particle fluxes. The data used here were obtained by the low-energy magnetosphere particle analyzer (LEMPA) subsystem, which cannot separate ion species. However, from data taken before switching into this mode, just outside the orbit of J4 when ion species were being separately identified and counted by the low-energy particle telescope (LEPT) subsystem, we know that the ratio of fluxes of heavy ions (oxygen and sulfur) to the fluxes of protons and helium was rapidly increasing with decreasing distance from Jupiter (2, 12). This would be expected in view of satellite contributions to the magnetosphere ion fluxes, such as the sputtering discussed here, and the volcanoes of Io (J1). The erosion rates discussed in this report are calculated as lower (upper) limits, assuming that all of the ions incident on a satellite surface are protons (oxygen).

Plotted in the inset to Fig. 1a are the differential ion fluxes $dJ(E)/dE$ (where J is the flux of ions of energy E) measured on Voyager 1 by LEMPA. These fluxes are used to calculate the water ice erosion flux $\Phi(\text{H}_2\text{O})$ ($\text{cm}^{-2} \text{sec}^{-1}$) for the satellites, assuming each is 50 percent ice-covered

$$\Phi_i(\text{H}_2\text{O}) = 0.5 \int_0^\infty \frac{dJ}{dE} S_i(E) dE d\Omega \quad (1)$$

where $S_i(E)$ is the laboratory water ice "sputtering" coefficient measured for incident ion species i . The proton erosion coefficient S_H increases from ~ 0.2 to ~ 2 for a decrease in incident proton energy from ~ 1.5 to ~ 0.1 MeV; it then decreases to ~ 0.8 for a proton energy of ~ 6 keV (6). The erosion coefficient varies as the square of the incident particle electronic energy loss $[(dE/dx)^2]$ in the water ice for energies greater than ~ 1 keV per atomic mass unit. At lower energies collision cascade dominates. The oxygen erosion coefficient S_O is $\sim 150 \times S_H$ in the energy region where both have been measured and is assumed to have the same $(dE/dx)^2$ energy dependence at the higher energies. The sputtering also increases rapidly with in-